2nd URSI AT-RASC, Gran Canaria, 28 May – 1 June 2018

A Statistical Survey of Radiation Belt Dropouts Observed by Van Allen Probes

Weichao Tu* (1), Zheng Xiang(1)(2), and Binbin Ni(2)
(1) Department of Physics and Astronomy, West Virginia University, Morgantown, West Virginia, USA
(2) Department of Space Physics, School of Electronic Information, Wuhan University, Wuhan, China

Abstract

Relativistic electron flux in the Earth's radiation belt are observed to drop by orders of magnitude on timescales of a few hours. Where do the electrons go? This is one of the most important outstanding questions in radiation belt studies. Here we perform statistical analysis on the radiation belt dropouts based on four years of electron phase space density data from Van Allen Probes. Our results show that the dropouts at larger L^* regions have higher occurrence, and cover a wider range in μ and K (the first the second adiabatic invariants) compared to those at low L^* regions. By comparing the statistical distribution of the dropout occurrence and ratio with the minimum resonant energy curve by EMIC waves, we find that EMIC wave scattering is the dominant loss mechanism at low L^* regions, while the dropouts at high L^* are due to a combination of EMIC wave scattering and outward radial diffusion associated with magnetopause shadowing, with outward radial diffusion leading to larger loss than EMIC wave scattering. The radiation belt dropouts at high L^* regions also have strong μ, K dependence. The electron variation at low μ and low K is dominated by fast injection or convection followed by fast decay, leading to very low occurrence of electron dropouts. However, at high μ, low K and other high K regimes, electrons suffer from abrupt dropouts and show high occurrence of dropouts at the high K regimes due to a combination of the two loss mechanisms.

1. Introduction

The Earth's radiation belts contain energetic electrons and protons that present a hazardous radiative environment for spacecraft operating within (e.g., [1, 2]). The relativistic electrons in the radiation belts are characterized by large variations in flux on various time scales [3, 4]. Recently, the NASA Van Allen Probes mission revealed two types of remarkable variations of outer belt electrons: the strong enhancement and fast dropout of flux by orders of magnitude on timescales of a few hours. Significant progress has been achieved in understanding the strong enhancement of relativistic electrons (e.g., [5, 6]). However, the mysterious fast dropout of relativistic electrons remains unsolved.

Where do the electrons go during the fast dropout? Radiation belt electrons can be lost either by transport across the magnetopause into interplanetary space, called magnetopause shadowing, or by precipitation into the atmosphere. Precipitation is caused by wave-particle interactions that induce pitch angle diffusion of electrons ([7] and references therein). Magnetopause shadowing occurs either due to the solar wind compression of the magnetopause or the outward radial diffusion of electrons (e.g., [8]). Thus, outward radial diffusion is another loss mechanism of relativistic electrons, which can not only transport electrons to the magnetopause but also decelerate electrons due to the conservation of the first adiabatic invariant. Outward radial diffusion is caused by electron drift resonance with Ultra-Low-Frequency (ULF) waves (e.g., [9]). It can be enhanced by intense ULF wave activities, and sharp radial gradient of electron distribution associated with magnetopause shadowing.

Even though various potential loss mechanisms for radiation belt dropouts have been identified, their relative contribution has not been resolved. For example, by analyzing data from THEMIS, GOES and NOAA/POES spacecraft, Turner et al. [8] suggested that the sudden electron depletion on 06 January 2011 was primarily caused by outward transport and magnetopause shadowing rather than precipitation. In contrast, Shprits et al. [10] showed that pitch angle diffusion by electromagnetic ion cyclotron (EMIC) waves was the dominant loss mechanism of ultra-relativistic electrons for the 17 January 2013 dropout. Recent results from our group on three distinct dropout events [11] suggested that the radiation belt dropouts can be classified into three types: magnetopause shadowing dominant, EMIC wave scattering dominant, and combination of both.

To systematically study the dominant loss mechanisms of radiation belt dropouts, statistical surveys of the dropout events that cover a variety of geomagnetic and solar wind conditions are required. Previous statistical studies of the radiation belt dropouts were mainly based on the electron flux observations (e.g., [12, 13]). However, to remove the adiabatic variations in the observed electron flux and reveal the real loss, we need to convert the flux data to electron Phase Space Density (PSD) as a function of the three adiabatic invariants (μ, K, L^*). Therefore, in this work we statistically analyze the dropouts in electron PSD and their dependence in μ, K, and L^*, to resolve the underlying loss mechanisms of radiation belt dropouts.

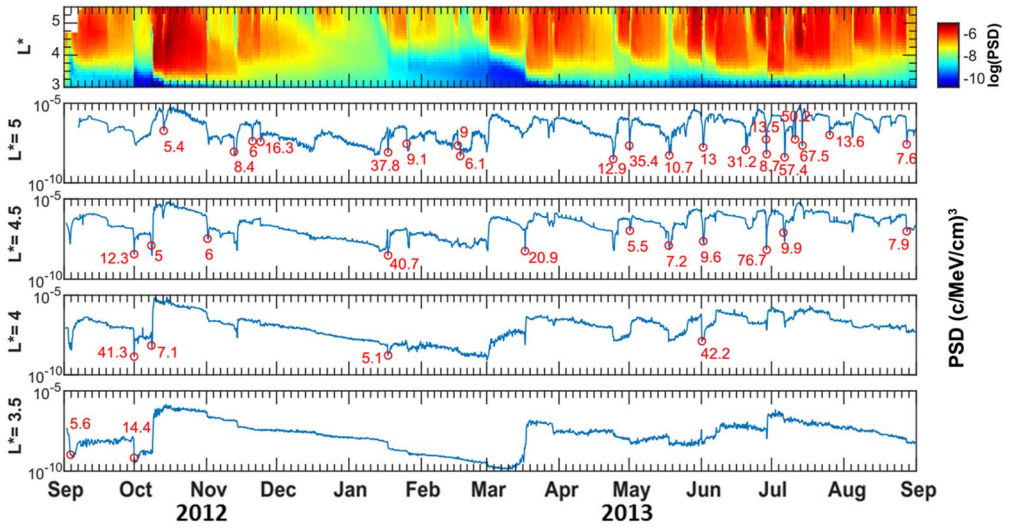

Figure 1. 1-year of electron PSD at μ = 1096 MeV/G and K = 0.172 $G^{1/2}R_E$, vs. L^* and time in the top panel and vs. time at different L^* values in the bottom panels. Dropout events are circled in red with the numbers denoting the dropout ratios.

2. Data and Method

Van Allen Probes data are ideally suited for this study since the observed electron flux cover a wide range of energies, pitch angles, and spatial distances. Here we convert four years (Sep 2012 to Sep 2016) of electron flux data from Van Allen Probes to PSD as a function of (μ, K, L^*) using the Tsyganenko 04 storm time model [14]. An example of the calculated PSD as a function of L^* and time at $\mu = 1096\ MeV/G$ and $K = 0.172\ G^{1/2}R_E$ are plotted in the top panel of Figure 1 for one year (Sep 2012-Sep 2013). The plot shows a variety of dropout events at different L^* regions. To identify the dropout events, we first bin the PSD data in L^* and time, and then at each L^* a dropout event is identified when the PSD is dropped by a factor >5 within a period <8 hours. For the period in Figure 1, PSD vs. time variation at $L^* = 5$ is plotted in the 2nd panel with the identified dropout events circled in red. The number by each circle is the dropout ratio to indicate how big is the dropout. Dropout events at lower L^* regions (L^* =4.5, 4, 3.5) are plotted in the following three panels. Based on the identified dropout events at different L^* regions, we find that there are more dropout events at higher L^* regions, while the dropout ratio is not necessarily higher at higher L^* (e.g., the large dropout at $L^* = 4$ near June 2013).

3. Results

After identifying all the dropout events based on four years of Van Allen Probes data, we statistically analyze the μ, K, and L^* dependence of the dropouts and plot the results in Figure 2. The top panels of Figure 2 show the number of dropout events versus μ and K at different L^* regions. Consistent with the results in Figure 1, there is higher dropout occurrence at higher L^* regions. In addition, we find the dropouts at high L^* regions cover a wider range of μ and K compared to low L^* regions. As a useful reference, in each panel of Figure 2 we over-plot a red curve which is the minimum resonant energy curve due to interactions with EMIC waves. The curve is calculated following the method and assumptions in Silin et al. [15] for different L^* regions. Theoretically, electrons located above the red curve can be efficiently scattering by EMIC waves, while the electrons below the curve cannot. The results show that at low L^* regions (e.g., L^*=3.5, 4), the dropout occurrence closely follows the red curve with most of the dropouts located above it. This suggest that EMIC wave scattering is the dominant loss mechanism at low L^* regions. However, at high L^* regions

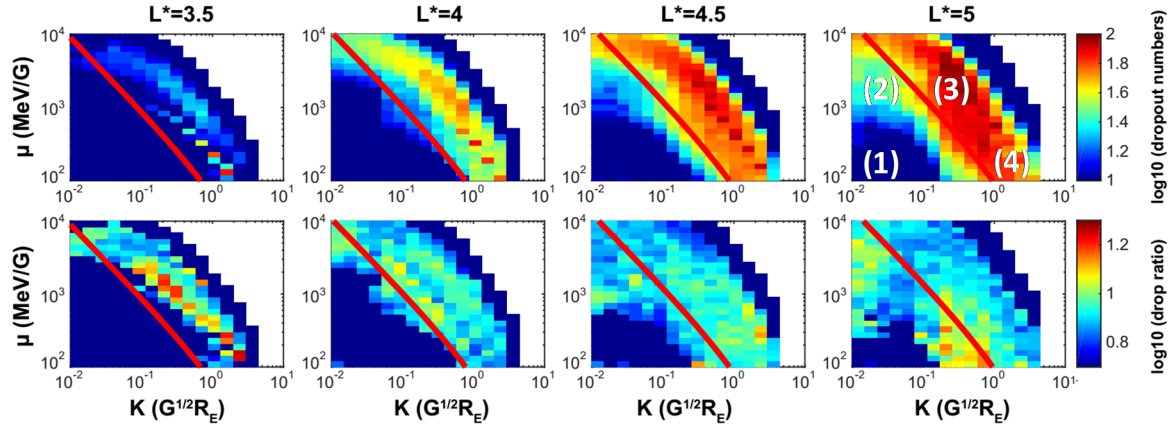

Figure 2. Distributions of dropout occurrence (top) and ratio (bottom) versus μ and K at different L^* regions. The red curves are the minimum resonant energy curves due to interactions with EMIC waves.

(e.g., L^* =4.5, 5), the results show significant dropout events both above and below the red curve, suggesting a combination of EMIC wave scattering loss and some other loss mechanisms that can also occur below the red curve. Statistically, we find the direct magnetopause shadowing loss is not significant at $L^* \leq 5$ since the last closed drift shell rarely reaches that low L^* regions. Therefore, the other contributing loss mechanism at high L^* regions that cover a wide range of (μ, K) is probably outward radial diffusion of electrons associated with magnetopause shadowing.

The bottom panels in Figure 2 shows the statistically averaged electron dropout ratio versus μ and K at different L^* regions. We find that above the red curve, the dropout ratio is higher at lower L^* regions, which indicates that the EMIC wave scattering loss is stronger at lower L^* regions. While for the dropouts below the red curve, the drop ratio is higher at higher L^*, which is consistent with faster outward radial diffusion at higher L^* regions associated with stronger magnetopause shadowing effects. Based on the dropout ratio distribution at L^*=5 (bottom right panel), we find the dropout ratio to be higher below the red curve than above, indicating that at high L^* regions, outward radial diffusion leads to larger dropout than EMIC wave scattering. To summarize, the statistical distributions of dropout occurrence and ratio in Figure 2 suggest that the dominant loss mechanism at low L^* regions is EMIC wave scattering, while the dropouts at high L^* regions are due to a combination of EMIC wave scattering and outward radial diffusion.

To further investigate the (μ, K) dependence of the dropouts, we mark four different (μ, K) regimes in the L^*=5 panel of Figure 2, with regime (1) being low μ, low K, (2) being high μ, low K, (3) being high μ, high K, and (4) being low μ, high K. One year of PSD data at the four (μ, K) regimes are plotted in Figure 3, with the top four panels showing the distributions of PSD vs. L^* and time. The plots show that at regime (1) low μ, low K, the PSD variation is mainly controlled by fast injection or convection followed by fast decay, probably due to scattering by hiss waves; while at the other three (μ, K) regimes, (2)-(4), the PSDs decay much slower but suffer from abrupt dropouts. The bottom four panels show the time variation of PSD at L^*=5 with identified dropout events. Consistent with the results in Figure 2, the least dropout events occur at regime (1), with the second least events at regime (2), and similar high occurrence of dropouts at regimes (3) and (4). The similar dropout responses at regimes (3) and (4) are probably due to the combination of EMIC wave scattering and outward radial diffusion above the red curve in Figure 2 at both regimes. Regime (2) has less dropout events since it is below the red curve and only outward radial diffusion can be effective there. However, why is regime (1) different from regime (2) considering they are both below the red curve? By looking at the two times marked in Figure 3 as

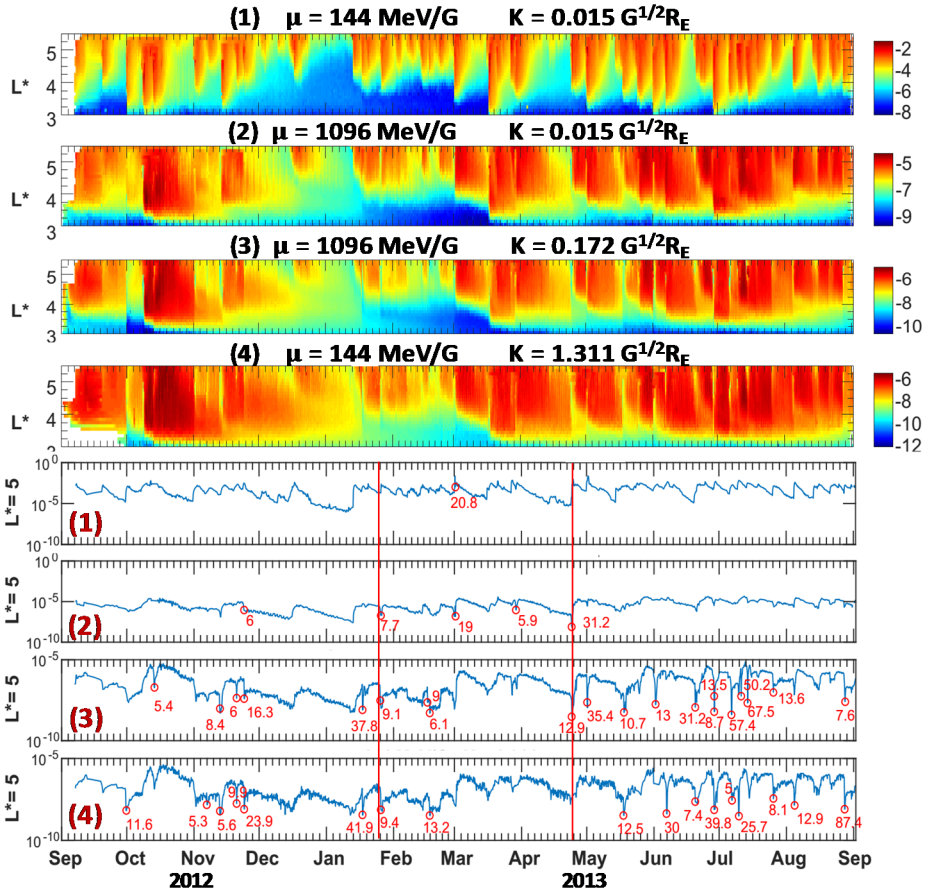

Figure 3. 1-year of electron PSD at four different (μ, K) values, versus L^* and time in the top panels and versus time at L^* =5 in the bottom panels.

examples (the red vertical lines), dropout events were identified at regimes (2), (3), and (4), while the PSD variations at regime (1) show a fast enhancement. Thus, the very low occurrence of dropouts at regime (1) low μ, low K is due to the concurrent fast injection or convection, which dominates over the loss effect.

4. Discussions and Conclusions

Based on four years of electron PSD data calculated from Van Allen Probes observations, we perform statistical analysis on the dropout occurrence and ratio at different μ, K, and L^* regimes and find that: 1. The dropout occurrence is higher at higher L^* regions, where the dropouts also cover a wider range of μ and K compared to the low L^* regions. 2. Using the minimum resonant energy curve due to EMIC waves as a reference, we conclude that EMIC wave scattering is the dominant loss mechanism at low L^* regions, while the dropouts at high L^* regions are due to a combination of EMIC wave scattering and outward radial diffusion associated with magnetopause shadowing. In addition, outward radial diffusion leads to larger dropout than EMIC wave scattering at high L^* regions. 3. At low μ, low K regime, electron PSD variations at high L^* regions are dominated by fast injection or convection followed by fast decay, showing very low occurrence of electron dropout. However, at high μ, low K and the other two high K regimes, PSD suffers from abrupt dropouts. The dropout occurrence is the highest at the high K regimes due to a combination of the two loss mechanisms. In the future, we will investigate the geomagnetic and solar wind conditions during the dropout events to further reveal the solar wind driver of the radiation belt dropouts.

5. Acknowledgements

This work was supported by NSF grant AGS-1613081 and NASA grant NNX15AW06G.

6. References

1. D. N. Baker, "Satellite anomalies due to space storms, in Space Storms and Space Weather Hazards," *NATO Sci. Ser. 2*, vol. **38**, edited by I. A. Daglis, 2001, pp. 285-311, Klouwer Acad., Dordrecht, Netherlands.

2. J. Allen, "The Galaxy 15 Anomaly: Another Satellite in the Wrong Place at a Critical Time," *Space Weather*, **8**, 6, 2010, doi:10.1029/2010SW000588.

3. G. D. Reeves, K. L. McAdams, R. H. W. Friedel, and T. P. O'Brien, "Acceleration and loss of relativistic electrons during geomagnetic storms," *Geophys. Res. Lett.*, **30**(10), 2003, 1529, doi:10.1029/2002GL016513.

4. D. N. Baker and S. Kanekal, "Solar cycle changes, geomagnetic variations, and energetic particle properties in the inner magnetosphere," J. *Atmos. Sol. Terr. Phys.*, **70**(2-4), 2008, 195-206, doi:10.1016/j.jastp.2007.08.031.

5. R. M. Thorne et al., "Rapid local acceleration of relativistic radiation-belt electrons by magnetospheric chorus," *Nature*, **504**, 2013, 411-414, doi: 10.1038/nature12889.

6. W. Tu, G. S. Cunningham, Y. Chen, S. K. Morley, G. D. Reeves, J. B. Blake, D. N. Baker, and H. Spence, "Event-specific chorus wave and electron seed population models in DREAM3D using the Van Allen Probes," *Geophys. Res. Lett.*, **41**, 2014, doi: 10.1002/2013GL058819.

7. R. M. Thorne, "Radiation belt dynamics: The importance of wave-particle interactions," *Geophys. Res. Lett.*, **37**, 2010, L22107, doi:10.1029/2010GL044990.

8. Drew L. Turner, Yuri Shprits, M. Hartinger, and V. Angelopoulos, "Explaining sudden losses of outer radiation belt electrons during geomagnetic storms," *Nature Physics*, 2012, doi:10.1038/nphys2185.

9. C. G. Fälthammar, "Effects of time-dependent electric fields on geomagnetically trapped radiation," *J. Geophys. Res.*, **70**, 1965, 2503.

10. Y. Y. Shprits et al., "Wave-induced loss of ultra-relativistic electrons in the Van Allen radiation belts," *Nat. Commun.*, **7**, 12, 2016, 883, doi: 10.1038/ncomms12883.

11. Z. Xiang, W. Tu, X. Li, B. Ni, S. K. Morley, and D. N. Baker, "Understanding the Mechanisms of Radiation Belt Dropouts Observed by Van Allen Probes," *Journal of Geophysical Research: Space Physics*, **122**, 10, October 2017, pp. 9858–9879, doi: 10.1002/2017JA024487.

12. H. Hietala, E. K. J. Kilpua, D. L. Turner, and V. Angelopoulos, "Depleting effects of ICME-driven sheath regions on the outer electron radiation belt," *Geophys. Res. Lett.*, 41, 2014, doi: 10.1002/2014GL059551.

13. C.-J. Yuan, Q.-G. Zong, W.-X. Wan, H. Zhang, and A.-M. Du, "Relativistic electron flux dropouts in the outer radiation belt associated with Corotating Interaction Regions," *J. Geophys. Res. Space Physics*, **120**, 2015, doi:10.1002/2015JA021003.

14. N. A. Tsyganenko and M. I. Sitnov, "Modeling the dynamics of the inner magnetosphere during strong geomagnetic storms," *Journal of Geophysical Research*, **110**, 2005, A03208, doi:10.1029/2004JA010798.

15. I. Silin, I. R. Mann, R. D. Sydora, D. Summers, and R. L. Mace, "Warm plasma effects on electromagnetic ion cyclotron wave MeV electron interactions in the magnetosphere," *J. Geophys. Res.*, **116**, 2011, A05215, doi:10.1029/2010JA016398.